Available online at www.sciencedirect.com
ScienceDirect
Journal of Organometallic Chemistry 693 (2008) 729–736
Journal of Organometallic Chemistry
www.elsevier.com/locate/jorganchem

Novel non-chelated cobalt(II) benzimidazole complex catalysts: Synthesis, crystal structures and cocatalyst effect in vinyl polymerization of norbornene

Naresh H. Tarte [a], Seong Ihl Woo [a,b,*], Liqiang Cui [a], Young-Dae Gong [c], Young Ho Hwang [d]

[a] Department of Chemical and Biomolecular Engineering (BK21 graduate program), Center for Ultramicrochemical Process System (CUPS), Korea Advanced Institute of Science and Technology, 373-1 Guseong-dong, Yuseong-gu, Daejeon 305-701, Republic of Korea
[b] Department of Chemistry, Korea Advanced Institute of Science and Technology, 373-1 Guseong-dong, Yuseong-gu, Daejeon 305-701, Republic of Korea
[c] Center for High Throughput Synthesis Technology, Korea Research Institute of Chemical Technology, Daejeon 305-600, Republic of Korea
[d] Daelim Daedeok R&D Center, Daejeon 305-345, Republic of Korea

Received 13 November 2007; received in revised form 27 November 2007; accepted 4 December 2007
Available online 8 December 2007

Abstract

The novel non-chelated monodentate benzimidazole (BI) complexes $CoCl_2(BI)_2$ (**1**)–(**3**), where BI = 1-(2-methoxybenzyl)- 2-(2-methoxyphenyl)-1*H*-benzimidazole (**1**), BI = 2-(2,6-difluorophenyl)-1*H*-benzimidazole (**2**) and 2-methyl-1*H*-benzimidazole (**3**) were synthesized and characterized by single X-ray crystallography. Unexpectedly, in solid state these complexes show similar coordination behavior to their analogue nickel(II) benzimidazole complexes such as inter-molecular *H*-bonding pattern and presence of acetonitrile solvent molecules per unit of complex molecule. Moreover, among these cobalt catalysts **1**–**3**, similar trend to that of nickel catalysts is observed for metal-to-nitrogen (M–X) coordination bond length and halogen–metal–halogen (X–M–X) bond angle. But unlike nickel(II) benzimidazole complexes, these catalysts show very low activity for vinyl polymerization of norbornene (NB) upon activation with methylaluminoxane (MAO); however, the activity abruptly increased in modified methylaluminoxane (MMAO). The presence of a small amount of toluene strongly hampered the activity, and the use of dry methylaluminoxane (dMAO) as a cocatalyst did not result in a high activity. The use of toluene-free solid modified methylaluminoxane (sMMAO) is found to be the best cocatalyst, where the highest activity of value 3.9×10^7 g of PNB mol_{Co}^{-1} h^{-1} was achieved for **3**/sMMAO at 30 °C.

Keywords: Non-chelated catalysts; Cobalt(II) catalysts; Norbornene polymerization; Cocatalyst effect; Benzimidazole ligand

1. Introduction

Polynorbornene *via* vinyl addition possesses special properties such as high thermal stability, high glass transition temperature (T_g), high transparency, and excellent dielectric properties that make them a good candidate as a coating material of optical disks and as inter-level dielectrics in the microelectronics industry [1]. The research on norbornene polymerization with early transition metal single-site catalysts has been directed to ring-opening metathesis polymerization [2] rather than vinyl polymerization because of their low activity for the latter.

After the discovery of nickel- and palladium-based catalysts by Brookhart et al. [3] and iron- and cobalt-based catalysts by Gibson et al. [4] for ethylene polymerization, intense work has been carried out for the discovery of nickel and cobalt based catalyst systems for α-olefin and cyclic olefins such as norbornene addition polymerization. Particularly, the nickel [5] and palladium [6] catalysts showed

* Corresponding author. Address: Department of Chemical and Biomolecular Engineering (BK21 graduate program), Center for Ultramicrochemical Process System (CUPS), Korea Advanced Institute of Science and Technology, 373-1 Guseong-dong, Yuseong-gu, Daejeon 305-701, Republic of Korea. Tel.: +82 42 869 3918; fax: +82 42 869 8890.
E-mail address: siwoo@kaist.ac.kr (S.I. Woo).

0022-328X/$ - see front matter © 2007 Elsevier B.V. All rights reserved.
doi:10.1016/j.jorganchem.2007.12.001

renewed interest due to high activity toward homopolymerization of norbornene. Generally, the polymerization activity drop in group VIII metals show the trend Co > Ni > Pd > Pt [7,5c], but the activity of cobalt-based catalyst for norbornene polymerization showed a high drop [8] and sometimes no activity compared to nickel at a given set of experimental conditions. Alt et al. [9] proposed highly active cobalt based catalysts for vinyl polymerization of norbornene in chlorobenzene but the activity was strongly hampered by the small amount of toluene present in commercial MAO and hence highest activity was achieved in MAO synthesized in chlorobenzene. This initiated us to investigate the effect of structure of MAO on norbornene polymerization using these cobalt catalysts.

Recently, we proposed [10] that nickel(II) monodentate benzimidazole complex catalysts in combination with MAO are the most active catalysts for vinyl polymerization of norbornene. Interestingly, we found that the cobalt(II) benzimidazole complexes show high structural analogy toward nickel(II) benzimidazole complexes at molecular level in solid state. Herein, we describe the structure of these cobalt(II) benzimidazole complexes and the effect of the cocatalyst on vinyl polymerization of norbornene by these catalysts.

2. Results and discussion

2.1. Preparation of the ligands and complexes

The ligands 1-(2-methoxybenzyl)-2-(2-methoxyphenyl)-1*H*-benzimidazole (MOBPBI) and 2-(2,6-difluorophenyl)-1*H*-benzimidazole (DFPBI) have been synthesized according to the reported procedure [10], whereas the ligand 2-methyl-1*H*-benzimidazole (MBI) is used as received from the commercial sources. The neutral benzimidazole cobalt derivatives [$CoCl_2$(MOBPBI)$_2$ (**1**)], [$CoCl_2$(DFPBI)$_2$ (**2**)] and [$CoCl_2$(MBI)$_2$ (**3**)] were prepared by reaction of $CoCl_2$ with the proper benzimidazole derivative in dichloromethane and purified by re-precipitation in diethyl ether. These complexes were dissolved in acetonitrile and the slow evaporation of solvent at room temperature yielded the fine crystals within a month. These complexes were isolated in the form of blue crystalline solid and are stable at room temperature. Due to low solubility of the complexes **1**–**2**, the ^{1}H NMR analyses was carried out in DMSO-d_6. The ^{1}H NMR spectra's are attributable to the protons of the respective derivative of benzimidazole ligand. Moreover, because of the broad nature of the ^{1}H NMR peaks, the methoxy proton peaks (O–CH_3; $\delta \sim 3.7$ and $\delta \sim 3.5$) of **1** could be overlapped by the DMSO-d_6 (δ 4–3) peak and hence are not seen in NMR spectra. Such broad NMR peak pattern suggests that there is a significant interaction between the benzimidazole ligands and the cobalt atom. This has been confirmed by the determination of their respective X-ray crystal structures which confirm the benzimidazole imine coordination with the metal center.

2.2. Molecular structures of cobalt benzimidazole complexes *1*–*3*

The X-ray crystal structures of complexes **1**–**3** are shown in Figs. 1–3, respectively. The crystallographic data and

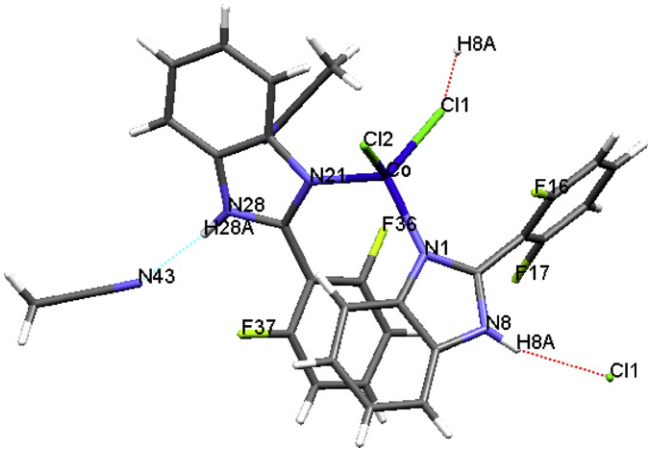

Fig. 2. X-ray structure of complex **2** showing inter-molecular *H*-bonding and acetonitrile solvent molecules.

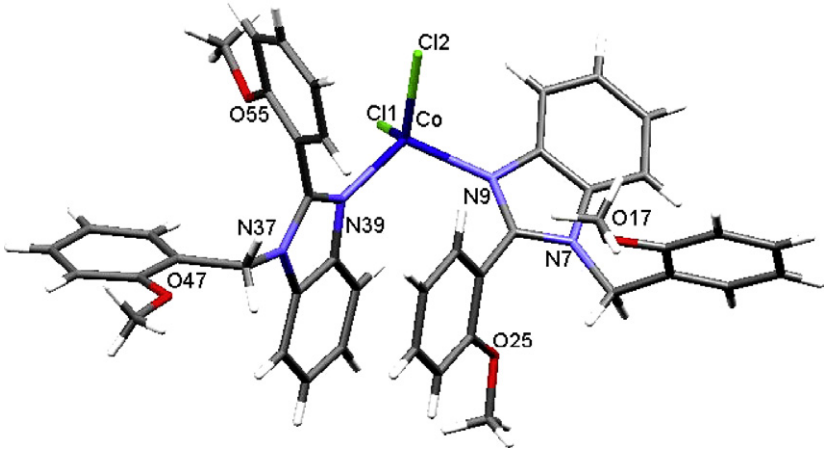

Fig. 1. X-ray structure of complex **1**.

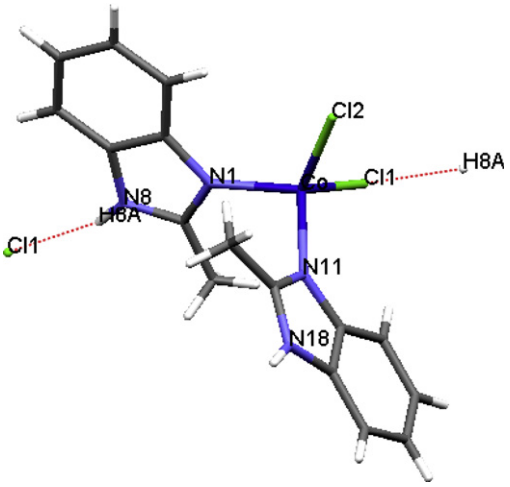

Fig. 3. X-ray structure of complex **3** showing inter-molecular *H*-bonding.

refinement parameters of complexes **1**–**3** are summarized in Table 1.

The coordination geometry around the cobalt is pseudo-tetrahedral similar observed to that of analogous nickel complexes [10]. The crystal structure of complex **2** consists of two solvent molecules per unit of the complex. Table 2 lists the relevant bond distances and angles of these cobalt benzimidazole complexes.

Complex **2** shows three types of inter-molecular *H*-bonding in solid state, one of which is between amide hydrogen of one of benzimidazole from first complex molecule and chloride atom of neighboring second complex molecule [N–H(8A)–Cl(1)]. Similarly, the chloride atom of first complex molecule involved in *H*-bonding with the amide hydrogen of third complex molecule [Cl(1)–N–H(8A)] and the third *H*-bonding is between the second benzimidazole amide hydrogen of first complex molecule and the nitrogen of solvent acetonitrile molecule [N–H(28A)–N(43)]. This indicate that each complex molecule is connected to two neighboring complex molecules and one acetonitrile molecule through inter-molecular *H*-bonding giving high stability to the 3D complex structure in solid state. Moreover, it also shows the presence of one discrete acetonitrile solvent molecules per unit of complex molecule in X-ray crystal. A similar pattern of *H*-bonding and the presence of solvent molecules have been seen in the analogue nickel complex [10].

Similar to analogue nickel complex, complex **3** (Fig. 3) shows inter-molecular *H*-bonding only with the chloride atom [N–H(8A)—Cl(1)]. The two Co–N bonds in complex

Table 1
Crystallographic data and structure refinement for complexes **1**, **2** and **3**

Parameter	$[CoCl_2(MOBPBI)_2$ (**1**)]	$[CoCl_2(DFPBI)_2$ (**2**)]	$[CoCl_2(MBI)_2$ (**3**)]
Empirical formula	$C_{44}H_{40}Cl_2Co\ N_4O_4$	$C_{30}H_{22}Cl_2CoF_4N_6$	$C_{16}H_{16}Cl_2CoN_4$
Formula weight	818.63	672.37	394.16
Temperature (K)	296(2)	296(2)	296(2)
Wavelength (Å)	0.71073	0.71073	0.71073
Crystal system	Monoclinic	Monoclinic	Monoclinic
Space group	*P*2(1)/*c*	*P*2(1)/*c*	*P*2(1)/*n*
Unit cell dimensions			
a (Å)	14.2536(10)	9.89690(10)	12.7017(3)
b (Å)	13.1213(9)	23.8815(3)	9.8602(2)
c (Å)	21.5173(15)	13.9141(2)	14.7287(3)
α (°)	90	90	90
β (°)	101.926(4)	110.069(10)	111.8680(10)
γ (°)	90	90	90
V (Å^3)	3937.4(5)	3088.95(7)	1711.91(6)
Z	4	4	4
D_{calc} (Mg/m^3)	1.381	1.446	1.529
Absorption coefficient (mm^{-1})	0.620	0.783	1.317
F(000)	1700	1364	804
Crystal size (mm^3)	0.27 × 0.20 × 0.07	0.22 × 0.20 × 0.08	0.26 × 0.23 × 0.04
θ Range for data collection (°)	1.46–28.30	1.71–28.31	1.81–28.39
Index ranges	$-18 \leqslant h \geqslant 18$, $-13 \leqslant k \geqslant 17$, $-28 \leqslant l \geqslant 26$	$-13 \leqslant h \geqslant 13$, $-31 \leqslant k \geqslant 30$, $-17 \leqslant l \geqslant 18$	$-16 \leqslant h \geqslant 16$, $-13 \leqslant k \geqslant 13$, $-19 \leqslant l \geqslant 19$
Reflections collected	40474	32304	17581
Independent reflections [R_{int}]	9762 [0.0430]	7674 [0.0572]	4270 [0.0255]
Completeness to theta = 28.30° (%)	99.7	99.8	99.3
Absorption correction	Multi-scan	Multi-scan	Multi-scan
Maximum and minimum transmission	0.9579 and 0.8504	0.9400 and 0.8466	0.9492 and 0.7257
Refinement method	Full-matrix least-squares on F^2	Full-matrix least-squares on F^2	Full-matrix least-squares on F^2
Data/restraints/parameters	9762/0/454	7674/0/ 390	4270/0/208
Goodness-of-fit on F^2	1.081	0.997	1.028
Final *R* indices [$I > 2\sigma(I)$]	$R_1 = 0.0750$, $wR_2 = 0.2136$	$R_1 = 0.0450$, $wR_2 = 0.0872$	$R_1 = 0.0308$, $wR_2 = 0.0826$
R indices (all data)	$R_1 = 0.1306$, $wR_2 = 0.2479$	$R_1 = 0.1263$, $wR_2 = 0.1112$	$R_1 = 0.0455$, $wR_2 = 0.0905$
Largest difference in peak and hole (e Å^{-3})	1.525 and −1.650	0.239 and −0.246	0.327 and −0.288

Table 2
Comparison of selected bond lengths (Å) and angles (°) for **1**–**3**

[$CoCl_2$(MOBPBI)$_2$ (**1**)]	[$CoCl_2$(DFPBI)$_2$ (**2**)]	[$CoCl_2$(MBI)$_2$ (**3**)]
Co–N(39)–2.038(3)	Co–N(21)–2.017(2)	Co–N(1)–2.0352(15)
Co–N(9)–2.063(3)	Co–N(1)–2.017(2)	Co–N(11)–2.0357(16)
Co–Cl(2)–2.2409(13)	Co–Cl(2)–2.2458(8)	Co–Cl(2)–2.2443(6)
Co–Cl(1)–2.2551(15)	Co–Cl(1)–2.2501(8)	Co–Cl(1)–2.2636(6)
N(39)–Co–N(9)–110.84(13)	N(21)–Co–N(1)–112.91(9)	N(1)–Co–N(11)–104.15(6)
N(39)–Co–Cl(2)–113.73(11)	N(21)–Co–Cl(2)–105.99(6)	N(1)–Co–Cl(2)–117.11(5)
N(9)–Co–Cl(2)–102.86(10)	N(1)–Co–Cl(2)–104.93(6)	N(11)–Co–Cl(2)–105.77(5)
N(39)–Co–Cl(1)–106.53(11)	N(21)–Co–Cl(1)–105.91(7)	N(1)–Co–Cl(1)–105.15(5)
N(9)–Co–Cl(1)–105.35(11)	N(1)–Co–Cl(1)–114.03(7)	N(11)–Co–Cl(1)–114.73(5)
Cl(2)–Co–Cl(1)–117.17(6)	Cl(2)–Co–Cl(1)–112.92(3)	Cl(2)–Co–Cl(1)–110.14(3)

1 [2.038(3) Å and 2.063(3) Å] are asymmetric, compared to that of complex **2** [2.017(2) Å and 2.017(2) Å] and complex **3** [2.0352(15) Å and 2.0357(16) Å]. Also the benzyl substitution results in the increase of Cl(1)–Co–Cl(2) bond angle in complex **1** [117.17°(6)] compared to the non-substituted complex **2** [112.92°(3)]. In the case of complex **3**, this angle further decreased to 110.14°(3). The analogue nickel benzimidazole complexes also show a similar trend in Ni–N bonding [**1**: 1.993 Å, 2.028 Å; **2**:1.993 Å, 1.987 Å; **3**:2.000 Å, 2.003 Å] and similar trend in Br(1)–Ni–Br(2) bond angle [**1**: (123.80°) > **2** (118.30°) > **3**(112.73°)]. All this indicates that the nucleation mechanism is common in both these cobalt and nickel benzimidazole complexes.

However, these bond angles are quite deviated from that of monodentate pyrazole derivatives of palladium [11] which is due to the geometric constraints as palladium can form only square planar complexes whereas these nickel and cobalt complexes show pseudo-tetrahedral geometry. These complexes are found to be stable at high temperature. The DSC–TGA analyses show that the first onset decomposition temperature is 230, 245 and 265 °C for complexes **1**–**3** which is in the similar range as reported for different cobalt benzimidazole derivatives [12].

2.3. Polymerization of norbornene

The results of polymerization of norbornene using cobalt complexes **1**–**3** with different kinds of methylaluminoxane are summarized in Table 3.

We have reported [10] that the nickel benzimidazole catalysts show very high activities for polymerization of norbornene in combination with MAO. Similar attempts to activate cobalt benzimidazoles using MAO were not successful and showed smallest activity values (runs 1, 6, and 10) for vinyl polymerization of norbornene. The reason can be attributed to the presence of toluene in commercial MAO which has already been noted for its inhabitation effect [9]. We have also reported for nickel benzimidazole catalysts that the use of toluene as the solvent in polymerization system dropped the activity drastically. Hence, to improve the polymerization activity, we carried out the polymerization in toluene-free environment by drying the MAO and using its solution in *o*-DCB. The results

Table 3
Cocatalyst dependence polymerization of norbornene by **1**–**3**[a]

Run	Catalyst	Cocatalyst	Time (min)	Yield (g)	Activity[b]	M_w ($\times 10^{-5}$)	M_w/M_n
1	**1**	MAO	30	0.02	0.008	nd[f]	
2	**1**	dMAO	30	0.67	0.27	5.2	2.6
3	**1**	MMAO	1/2	0.57	13.68	7.1	2.7
4	**1**	sMMAO	1/2	0.88	21.12	4.5	2.8
5[c]	1	dMAO	5		NA[d]		
6	**2**	MAO	30	0.03	0.012	nd[f]	
7	**2**	dMAO	30	0.39	0.16	5.8	2.6
8	**2**	MMAO	1/2	0.76	18.24	8.1	3.4
9	**2**	sMMAO	1/2	0.80	19.2	4.5	2.9
10	**3**	MAO	5	0.72	1.73	ns[g]	
11	**3**	MMAO	1/2	0.77	18.48	9.0	3.3
12	**3**	sMMAO	1/2	0.94	22.56	4.6	3.4
13[e]	3	sMMAO	1/2	1.63	39.12	5.6	2.9
14	**3**	dMAO	5	0.54	1.29	7.6	2.8
15	**3**	dMAO/TMA	1	0.81	9.72	6.6	2.8
16	**3**	sMMAO/TIBA	5		NA[d]		

[a] *Conditions*: Cobalt precatalyst: 5.0 μmol, Al/Co: 500, temp.: 30 °C, Norbornene (Nb): 10.0 mmol, solvent: *o*-DCB, total volume: 15 mL.
[b] Activity: 10^6 g PNB mol^{-1} h^{-1}.
[c] In 2:1 *o*-DCB/toluene.
[d] NA: not active.
[e] Nb: 25.0 mmol, Al/Co: 1000.
[f] nd: not determined.
[g] ns: polymer not soluble in 1,2,4-trichlorobenzene.

improved the activity for **1**–**2**/dMAO (runs 2 and 7), but in the case of **3**/dMAO (runs 10 and 14) the activity dropped compared to **3**/MAO. However, the increased activity in dMAO/Me_3Al (run 15) indicates that free Me_3Al available in cages of dMAO was not sufficient for the activation of complex **3**. The alternative use of MMAO (runs 3, 8 and 11) in toluene showed very high activity compared to MAO and dMAO, which indicates that the microstructure of the cocatalyst plays a major role in generating and stabilizing the highly mature active species which is responsible for higher activity. However, the relatively high activity for MAO and dMAO activation for **3** (runs 10 and 14) than **1** (runs 1–2) and **2** (runs 6–7) may be due to the electronically poor ligand [10] which makes the cobalt less cationic and hence fewer the aluminium to

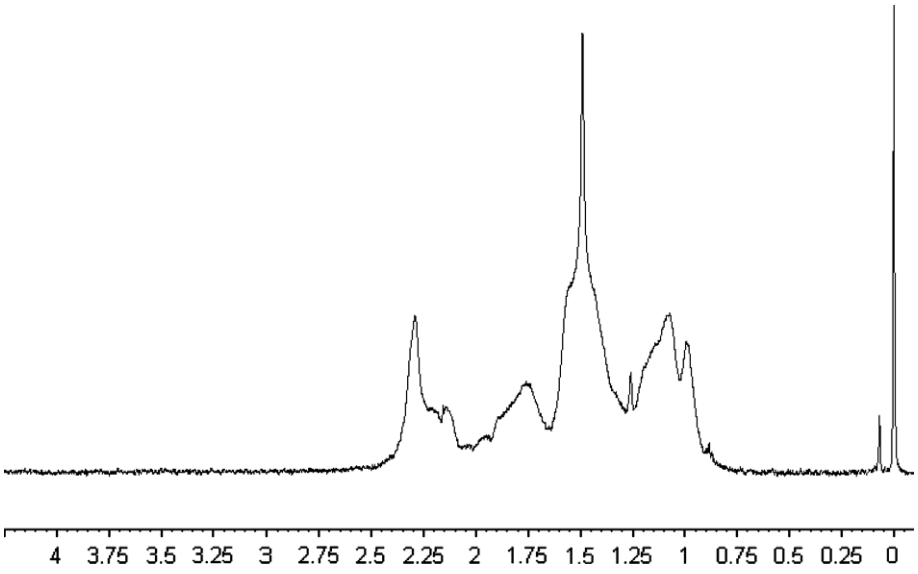

Fig. 4a. ^{1}H NMR spectra of polynorbornene produced by **1**/MMAO.

cobalt interactions and less the possibility of bimetallic species formation [13] which can be the reason for low activity in **1**/MAO (run 1) and **2**/MAO (run 6).

In the case of MMAO, the drying process is not necessary because $^{i}Bu_3Al$ cannot form the bimetallic species with the active metal complex [13]. However, the presence of toluene can hamper the activity and hence we prepared toluene-free MMAO, i.e., sMMAO and used in *o*-DCB. It is observed that for all the catalysts, the highest activity was achieved using sMMAO (runs 4, 9, and 12), whereas **3**/sMMAO (run 13) represents the highest activity of value 3.9×10^7 g of PNB mol_{Ni}^{-1} h^{-1} within 30 s of polymerization with norbornene to cobalt ratio of 5000. It is interesting to note that the activity trend in cobalt benzimidazole catalysts is different to that of nickel benzimidazole catalysts, where in the earlier case **3**/sMMAO and in the latter case **1**/MAO was found to be the most active catalyst. However, among the cocatalysts used, the highest molecular weight was achieved using MMAO and a very high M_w of value 9.0×10^5 g mol^{-1} was observed for PNB produced by **3**/MMAO (run 11). This data indicate that the sMMAO is the best choice as cocatalyst for polymerization using this class of cobalt catalysts.

2.4. Polymer microstructure

The ^{1}H NMR spectrum of PNB produced by **1**/MMAO is presented in Fig. 4a.

The assignments of methylene and methine carbons were carried out on the basis of ^{13}C NMR analysis in combination with DEPT analysis (Figs. 4b and 4c) and based on previous reports [14]. The peaks between 53 and 37 ppm are assigned as methine carbon peaks and from 37 to 28 ppm are assigned as methylene carbons peaks. In PNB produced by **1**/MMAO, two peaks of non-equal intensity are observed for C7. Again, on the basis of assignments for hydrotrimers

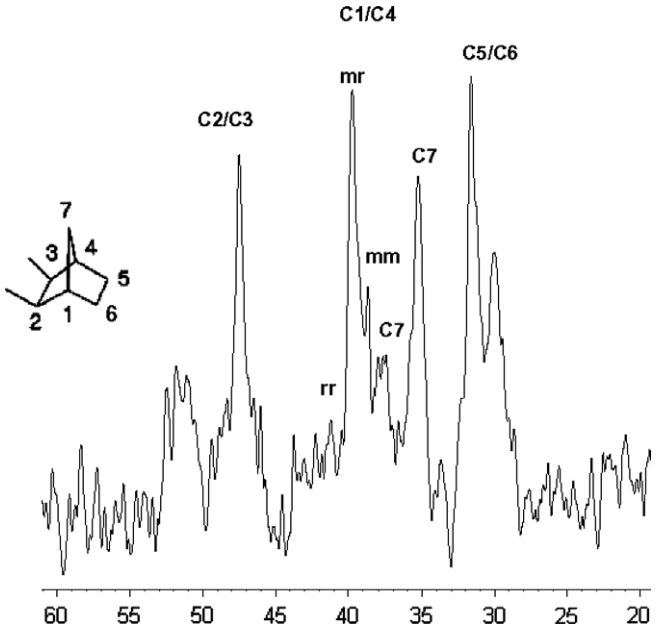

Fig. 4b. ^{13}C NMR spectra of polynorbornene produced by **1**/MMAO.

of norbornene by Arndt et al. [14] and reports from Bearns et al. [15], one would expect two peaks for C7 if the polynorbornene enchainment was divided between *mm* and *mr* placements or between *rr* and *mm*. Two major peaks were observed below 40 ppm for C1 and C4 for PNB produced by **1**/MMAO. According to Arndt et al. [14], only the *mm* and *mr* triads of the hydrotrimers of norbornene exhibit C1 and C4 resonances below 40 ppm. Additionally, C7 in the *mm* norbornene triad resonates at 33.82 ppm, 34.30 ppm in the *rr* triad, and 34.12 ppm in the *mr* triad. Thus one would expect a mixture of *mm* and *mr* or *mm* and *rr* to be resolved sufficiently to yield two peaks.

The resonance of C7 carbon (Figs. 4b and 4c) which is the region between 37 and 34 ppm shows two peaks, the one at

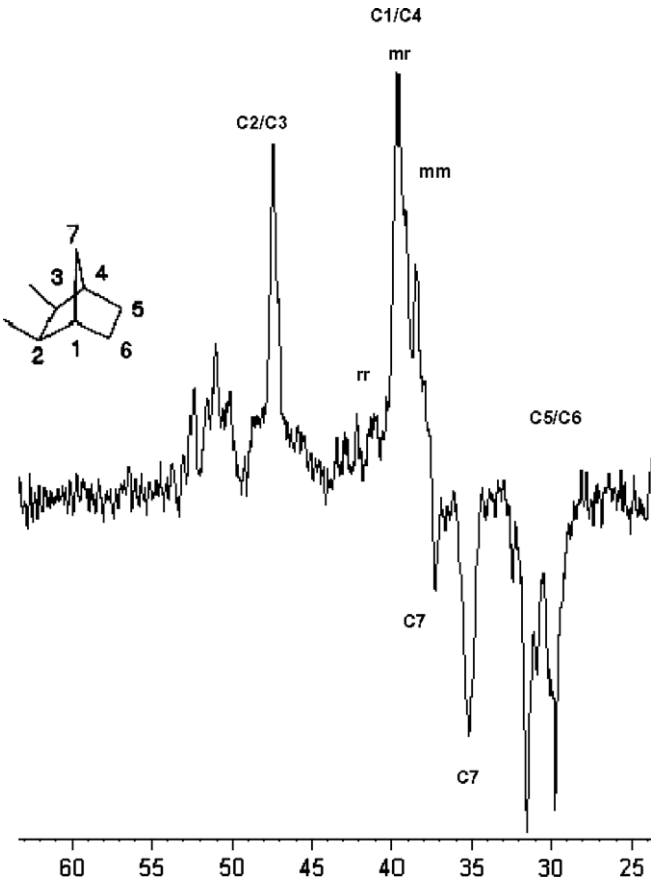

Fig. 4c. ^{13}C DEPT NMR spectra of polynorbornene produced by **1**/MMAO.

34.3 ppm and the other at 36.9 ppm in which the intensity of earlier peak is very strong to that of latter. Thus the microstructure of PNB produced by **1**/MMAO can be best described as a mixture of *mm* and *mr* triads in which *mm* is highly populated. The presence of the shoulder peak near 39 ppm which is reported as the C1 and C4 peaks of the central norbornene of the *mm* triad of hydronorbornene trimers by Arndt et al. [14] supports the high population of *mm* triads in the polynorbornene. The polynorbornene produced by **1**/MMAO shows a typical WAXS pattern, and one additional broad and weak intense peak at $2\theta = 30.12°$ which proves that the higher crystalline nature of PNB which may be due to comparatively higher fraction of syndiotactic microstructure. Such increased tacticity increases the permeability coefficient [16]. This polynorbornene shows high glass transition temperature (T_g) of value 465 °C, which is in consistence with the T_g reported for PNB produced by these catalyst [10] upon activated with MAO. A similar high value T_g are reported for PNB's produced by neutral salicylaldiminato Ni(II) complexes [5a].

3. Conclusions

It is observed that the non-chelated cobalt(II) benzimidazole complexes show similar coordination behavior with its nickel counterpart but failed to produce similar catalytic activity for vinyl polymerization of norbornene in combination with MAO. The use of modified methylaluminoxane (MMAO) abruptly increased the polymerization activity, but a small amount of toluene present in the polymerization system strongly hampers the catalyst performance and hence toluene-free MMAO, i.e. sMMAO is found to be the best cocatalyst for activation of these cobalt benzimidazole catalysts. Moreover, the activity trend among these cobalt catalysts also differs to the nickel series, as in the case of cobalt series **3**/sMMAO showed highest activity values for vinyl polymerization of norbornene.

4. Experimental

4.1. General procedures

All procedures were carried out by using standard Schlenk techniques. 1,2-Dichlorobenzene (anhydrous grade) and cobalt(II) chloride were purchased from Aldrich and were used without any further purification. Methylaluminoxane (MAO; Aldrich) was obtained as 10 wt% and MMAO (Akzo Nobel) as 7.25 wt% solutions in toluene and were used without further treatment. The dMAO was prepared under reduced pressure according to the reported procedure [17] and a similar procedure was followed to prepare sMMAO. 2-Methylbenzimidazole was purchased from Fluka (98%). Norbornene (bicyclo-[2.2.1]hept-2-ene; Aldrich) was purified by distillation over potassium and was used as a solution in *o*-DCB just prior to polymerization.

4.2. Measurement

NMR spectra of ligands were recorded using $CDCl_3$ and complex using DMSO-d_6 as solvents on a Bruker BMX-500 MHz instrument with tetramethylsilane (TMS) as the internal standard. The ^1H NMR data of polynorbornene were recorded at ambient temperature and the ^{13}C NMR data was recorded at 100 °C using 1,2-dichlorobenzene-d_4 as solvent on a Bruker AMX-500 MHz spectrometer. The FT-IR analyses of polynorbornene produced by **1**–**3** were carried out using ATR-FTIR spectrometer (Sens IR). The combine differential scanning calorimeter-thermogravimetric analysis (DSC–TGA) was carried out under nitrogen using Setsys 16/18 (SETRAM) instrument and the DSC data were obtained under nitrogen up to 500 °C with a heating rate of 10 °C/min using NETZSCH DSC-204F1. Molecular weight and molecular weight distribution of polynorbornene were measured by gel permentation chromatography (GPC) (PL-GPC 220) at 160 °C using 1,2,4-trichlorobenzene as solvent and calibrated using polystyrene standards. Elemental analysis was carried out by Faison's elemental analyzer-1110. The melting points of ligands were measured by electrical apparatus with Mettler Toledo FP90 Control Processor.

4.3. Syntheses

All ligands were synthesized according to the reported procedures [10] and the complex syntheses were carried out under nitrogen atmosphere.

4.3.1. Synthesis of 1-(2-methoxybenzyl)-2-(2-methoxyphenyl)-1H-benzimidazole (MOBPBI)

The solution of 1,2-diaminobenzene (1.08 g, 10.0 mmol) and stoichiometric amount of sodium acetate in glacial acetic acid (30 mL), was added dropwise to the solution of *o*-anisaldehyde (2.86 g, 21.0 mmol) in glacial acetic acid (50 mL). After complete addition at room temperature, the resultant mixture was set to reflux for 21 h. The reaction mixture was cooled to room temperature, evaporated in vacuum, and partitioned between dichloromethane and water. The biphasic mixture was cooled in an ice bath, and neutralized with solid potassium carbonate with vigorous stirring. The phases were separated, and the extraction was completed with additional portions of dichloromethane. The combined organic extracts were dried with Na_2SO_4, and evaporated in vacuum. Purification by column chromatography (silica gel, *n*-hexane/ethyl acetate, 10/1) produced the title compound in 75% (2.58 g) yield. Melting point 151 °C. ^{1}H NMR (500 MHz, $CDCl_3$) δ 7.84 (d, 1H); 7.53 (m, 1H); 7.51 (m, 1H); 7.25–7.17 (m, 4H); 7.03 (t, 1H); 6.93 (d, 1H); 6.81 (d, 1H); 6.75 (t, 1H); 6.69 (dd, 1H); 5.23 (s, 2H); 3.76 (s, 3H); 3.56 (s, 3H). ^{13}C NMR (500 MHz, $CDCl_3$) δ 157.6, 156.5, 143.3, 135.5, 132.4, 131.4, 128.4, 127.7, 124.5, 122.5, 121.9, 120.8, 120.4, 119.8, 119.8, 110.9, 110.6, 109.9, 55.1, 55.2, 55.1, 43.5 ppm.

4.3.2. Synthesis of 2-(2,6-difluorophenyl)-1H-benzimidazole (DFPBI)

The 2,6-difluorobenzoyl chloride (1.94 g, 11.0 mmol) was dissolved in dichloromethane (20 mL), and was added dropwise over 1 h to a solution of 1,2-diaminobenzene (1.08 g, 10.0 mmol) and triethylamine (1.9 mL, 13.5 mmol) in dichloromethane (100 mL) at 0 °C. The reaction mixture was stirred at 0 °C for 1 h, then the temperature was set to room temperature while stirring continued over next 3 h, the volatiles were removed in vacuum to produce a pale yellow solid. The solid was dissolved in glacial acetic acid (50 mL), sodium acetate (0.90 g, 11.0 mmol) was added, and the mixture was refluxed for 21 h. Further treatment similar to (MOBPBI) produced the title compound (1.9 g, 82%) as a white solid. Melting point 202 °C. ^{1}H NMR (500 MHz, $CDCl_3$) δ 10.16 (br, 1H), 7.90 (br, 2H), 7.50 (m, 1H), 7.39–7.31 (m, 2H), 7.06 (m, 2H). ^{13}C NMR (500 MHz, DMSO-d_6) δ 109, 112, 118, 122, 132–134, 141–143, 159, 161 ppm.

4.3.3. Synthesis of [$CoCl_2$ (MOBPBI)$_2$ (**1**)]

Well-stirred solution of 0.76 g (2.2 mmol) of MOBPBI in dichloromethane (10 mL) was added dropwise to a solution of cobalt(II) chloride (0.13 g, 1.0 mmol) in dichloromethane (20 mL). A color change from faint pink to a sky blue was observed yielding a dark sky blue precipitate after stirring for 2 h at room temperature and filtered through a glass filter. The filtrate was evaporated in vacuum; the solid was washed frequently with diethyl ether to yield the title complex as sky blue solid. Crystallization in acetonitrile yields the title compound with 92% (0.75 g) yield. ^{1}H NMR (500 MHz, DMSO-d_6) δ 8.73–8.17 (br, 1H); 7.99–7.34 (br, 9H); 7.34–6.98 (br, 12H); 6.98–6.66 (dd, 3H); 6.66–6.46 (d, 1H); 5.68–5.03 (br, 2H). Anal. Calc. for $C_{44}H_{40}Cl_2CoN_4O_4$: C, 64.55; H, 4.92; N, 6.84. Found: C, 64.21; H, 4.63; N, 6.59%.

4.3.4. Synthesis of [$CoCl_2$ (DFBPI)$_2$ (**2**)]

A procedure similar to that for **1** produced dark blue crystals in acetonitrile. Yield: 82% (0.48 g). ^{1}H NMR (500 MHz, DMSO-d_6) δ 13.33–12.62 (br, 2H), 7.87–7.50 (br, 6H), 7.50–7.14 (br, 8H). Anal. Calc. for $C_{26}H_{16}Cl_2CoF_4N_4 \cdot 2CH_3CN$: C, 53.59; H, 3.30; N, 12.50. Found: C, 53.45; H, 3.11; N, 12.81%.

4.3.5. Synthesis of [$CoCl_2$(MBI)$_2$ (**3**)]

A procedure similar to that for **1** produced a violet crystalline solid was obtained with 88% (0.35 g) yield. Anal. Calc. for $C_{16}H_{16}Cl_2CoN_4$: C, 48.75, H, 4.09; N, 14.21. Found: C, 49.20; H, 4.27; N, 14.35%.

4.4. X-ray structural determination

The X-ray structure analyses data were collected using a Bruker SMART Apex II X-ray diffractometer, and the structure, solution and refinement were performed by using the SHELXS program [18].

4.5. General procedure for the polymerization of norbornene

The polymerization was carried out in a 100 mL glass reactor using *o*-DCB as the solvent at 30 °C. In a typical polymerization (run 3, Table 3), 5.0 μmol of precatalyst **1** was dissolved in *o*-DCB (10.0 mL) under nitrogen atmosphere, and freshly prepared solution of norbornene (1.5 mL, 10.0 mmol) in *o*-DCB was added. The polymerization was initiated by adding a toluene solution of MMAO (1.15 mL, 2.5 mmol). The highly viscous mass of polymer was observed in a very short period after the MAO addition. Hence the polymerization was terminated within 30 s by adding acidified methanol (20 mL, 5 mol% HCl). The polymer was isolated by filtration, washed with methanol, and dried in vacuum at 100 °C for 24 h. Unless otherwise stated, the total volume was 15 mL, which was achieved by variation of amount of *o*-DCB when necessary. All the polymers were characterized by IR and NMR and were found to be vinyl-type polynorbornene exclusively.

Acknowledgements

This research was funded by the Center for Ultramicrochemical Process Systems (CUPS) sponsored by KOSEF

(2006). We thank Dr. C.-H. Kim at Korea Research Institute of Chemical Technology, and Dr. J.-W. Shin at Korea Advanced Institute of Science and Technology for their technical assistance.

Appendix A. Supplementary material

CCDC 661666, 661667 and 661668 contain the supplementary crystallographic data for this paper. These data can be obtained free of charge from The Cambridge Crystallographic Data Centre via www.ccdc.cam.ac.uk/data_request/cif. Supplementary data associated with this article can be found, in the online version, at doi:10.1016/j.jorganchem.2007.12.001.

References

[1] N.R. Grove, P.A. Kohl, S.A. Bidstrup- Allen, S. Jayaraman, R. Shick, J. Polym. Sci., Part B: Polym. Phys. 37 (1999) 3003, and references therein.
[2] (a) K.J. Ivin, J.C. Mol, Olefin Metathesis and Metathesis Polymerization, Academic Press, San Diego, 1997, pp. 407;
(b) R.H. Grubbs, Comprehensive Organometallic Chemistry, vol. 8, Pergamon Press, Oxford, 1982, p. 499;
(c) C. Janiaks, in: E. Riedel, de Gruyter (Ed.), Moderne Anorganische Chemie, Berlin, 1998, p. 708.
[3] L.K. Johnson, C.M. Killian, M. Brookhart, J. Am. Chem. Soc. 117 (1995) 6414.
[4] G.J.P. Britovsek, M. Bruce, V.C. Gibson, B.S. Kimberley, P.J. Maddox, S. Mastroianni, S.J. McTavish, C. Redshaw, G.A. Solan, S. Strolmberg, A.J.P. White, D.J. Williams, J. Am. Chem. Soc. 121 (1999) 8728.
[5] (a) W.-H. Sun, H. Yang, Z. Li, Y. Li, Organometallics 22 (2003) 3678;
(b) H. Yang, W.-H. Sun, F. Chang, Y. Li, Appl. Catal. A 252 (2003) 261;
(c) C. Janiak, P.-G. Lassahn, Macromol. Rapid Commun. 22 (2001) 479, and reference therein.
[6] (a) A.D. Hennis, J.D. Polley, G.S. Long, A. Sen, D. Yandulov, J. Lipian, G.M. Benedikt, L.F. Rhodes, J. Huffman, Organometallics 20 (2001) 2802;
(b) P.-G. Lassahn, V. Lozan, B. Wu, A.S. Weller, C. Janiak, Dalton Trans. (2003) 4437;
(c) P.-G. Lassahn, V. Lozan, C. Janiak, Dalton Trans. (2003) 927.
[7] X. Zhana, M. Yang, Z. Lei, J. Mol. Catal. A: Chem. 184 (2002) 139.
[8] F. Bao, X. Lu, Y. Qiao, G. Gui, H. Gao, Q. Wu, Appl. Organomet. Chem. 19 (2005) 957.
[9] F.P. Alt, W. Heitz, Macromol. Chem. Phys. 199 (1998) 1951.
[10] N.H. Tarte, H.-Y. Cho, S.I. Woo, Macromolecules 40 (2007) 8162.
[11] K. Li, J. Darkwa, I.A. Suzie, S.F. Mapolie, J. Organomet. Chem. 660 (2002) 108.
[12] W.H. Sun, C. Shao, Y. Chen, H. Hu, R.A. Sheldon, H. Wang, X. Leng, X. Jin, Organometallics 21 (2002) 4350.
[13] (a) A. Ioku, T. Hasan, T. Shiono, T. Ikeda, Macromol. Chem. Phys. 203 (2002) 748;
(b) R. Kleinschmidt, Y. Leek, M. Reffke, G. Fink, J. Mol. Catal. A: Chem. 148 (1999) 29.
[14] M. Arndt, R. Engehausen, W. Kaminsky, K. Zoumis, J. Mol. Catal. A: Chem. 101 (1995) 171.
[15] D.A. Barnes, G.M. Benedikt, B.L. Goodall, S.S. Huang, H.A. Kalamarides, S. Lenhard, L.H. McIntosh III, K.T. Selvy, R.A. Shick, L.F. Rhodes, Macromolecules 36 (2003) 2623.
[16] T. Steinhausler, W.J. Koros, J. Polym. Sci., Part B: Polym. Phys. 35 (1997) 91.
[17] T. Hasan, K. Nishii, T. Shiono, T. Ikeda, Macromolecules 35 (2002) 8933.
[18] (a) G.M. Sheldrick, SHELX-97, A Computer Program for Crystal Structure Solution and Refinement, Universitat Gottingen, Gottingen, Germany, 1997;
(b) Sheldrick, G., SHELXTL-PC Release 4.1 Siemens Analytical X-ray Instruments, Inc., Madison, WI, 1990, p. 296.